Electronic Supplementary Material (ESI) for Journal of Materials Chemistry A

High-throughput screening of small-molecule adsorption in MOF

— Supplementary Materials —

Pieremanuele Canepa, Calvin A. Arter, Eliot M. Conwill, Daniel H. Johnson, Brian A. Shoemaker, Karim Z. Soliman, and T. Thonhauser

Department of Physics, Wake Forest University, Winston-Salem, NC 27109, USA.
(Dated: August 12, 2013)

I. MOF-74-$\mathcal{M}$ LATTICE CONSTANTS AND OTHER QUANTITIES

TABLE I. Computed lattice constants a and c (in Å) and volume V (in Å^3). Atomic numbers Z and Bader charges $Q_{\mathcal{M}}$ (in units of e) at the metal sites $\mathcal{M}$ are also reported. Experimental and computational data is reported in parenthesis where available.

$\mathcal{M}$	Z	a		c		V		$Q_{\mathcal{M}}$
Be	4	25.655		6.663		3797.877		1.6
Mg	12	26.084	(25.881)[a,1]	6.863	(6.878)	4043.947	(3990.357)	1.5
Al	13	25.402		6.565		3668.630		2.6
Ca	20	25.454	(26.759)[b,2]	7.591	(7.682)	4259.190	(4763.703)	1.5
Sc	21	23.675	(24.342)[b,2]	7.334	(7.247)	3559.960	(3718.993)	1.9
Ti	22	23.669	(26.477)[b,2]	7.210	(6.927)	3498.429	(4205.462)	1.8
V	23	25.254	(25.933)[b,2]	7.000	(6.943)	3868.982	(4043.558)	1.6
Cr	24	26.171	(26.329)[b,2]	6.525	(6.607)	3870.148	(3966.526)	1.5
Mn	25	26.242	(26.230)[a,3]	7.082	(7.035)	4223.524	(4191.711)	1.4
Fe	26	26.010	(26.098)[a,4]	6.711	(6.851)	3931.742	(4041.3)	1.3
Co	27	26.078		6.872		4047.173		1.3
Ni	28	25.688	(25.786)[a,5]	6.188	(6.770)	3536.291	(3898.3)	1.1
Cu	29	26.271		6.138		3668.332		0.8
Zn	30	26.142	(25.932)[b,6]	6.875	(6.836)	4068.779	(3981.5)	1.2
Sr	38	26.683		6.710		4137.427		1.6
Zr	40	23.455		7.530		3587.630		2.0
Nb	41	27.031		6.414		4058.779		1.4
Ru	44	27.061		6.119		3880.592		1.3
Rh	45	25.833		6.804		3932.355		1.3
Pd	46	26.570		6.432		3932.482		1.1
La	57	26.672		6.431		3962.091		2.2
W	74	26.960		6.177		3888.314		1.6
Os	76	26.480		4.977		3022.272		1.8
Ir	77	26.020		6.796		3984.552		1.2
Pt	78	26.560		6.511		3977.779		1.2

[a]Experimental data.
[b]Computational data GGA+D Grimme.

II. SIMULATED X-RAY POWDER DIFFRACTION SPECTRA

Figures 1, 2, 3, and 4 depict the simulated X-ray powder diffraction patterns of the four MOF-74-$\mathcal{M}$ with $\mathcal{M}$ = Pd, Os, Ir, and Pr, relevant for their future synthesis.

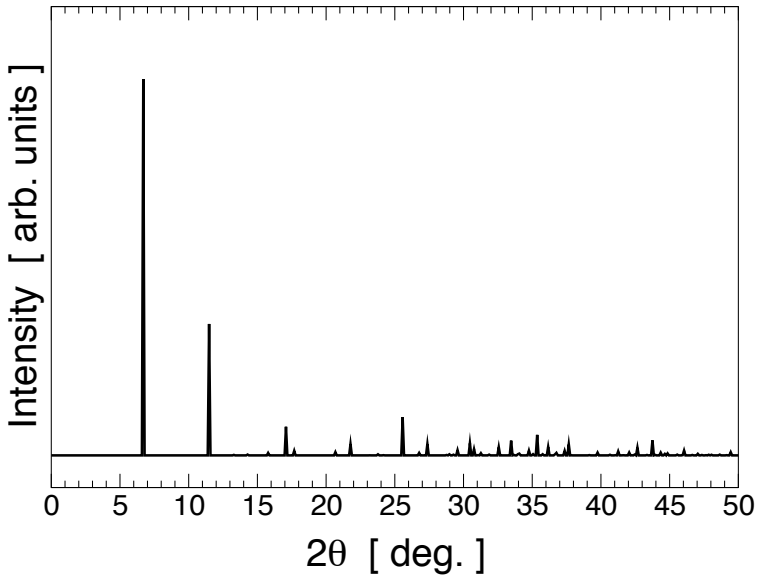

FIG. 1. X-ray powder diffraction pattern for MOF-74-Pd, using a Cu K source.

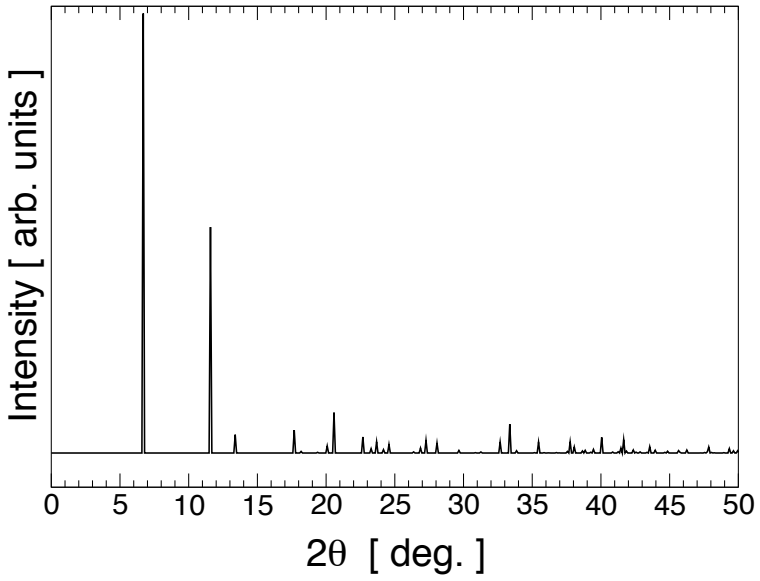

FIG. 2. X-ray powder diffraction pattern for MOF-74-Os, using a Cu K source.

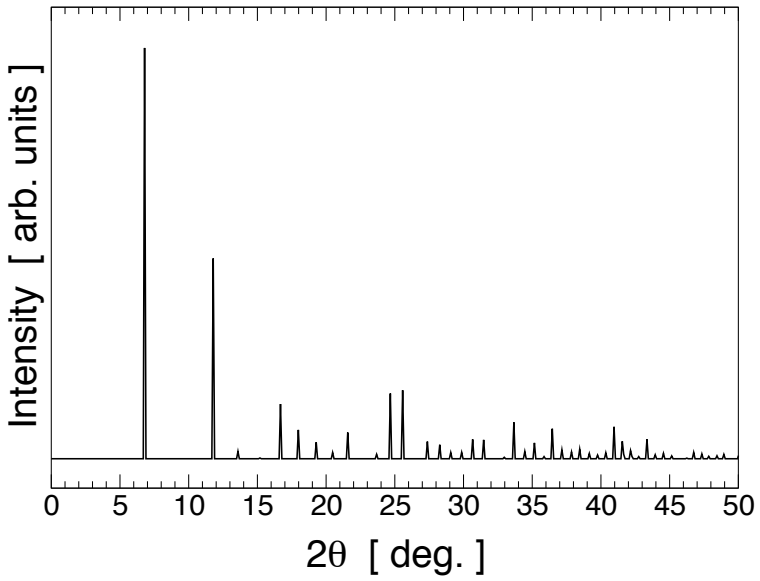

FIG. 3. X-ray powder diffraction pattern for MOF-74-Ir, using a Cu K source.

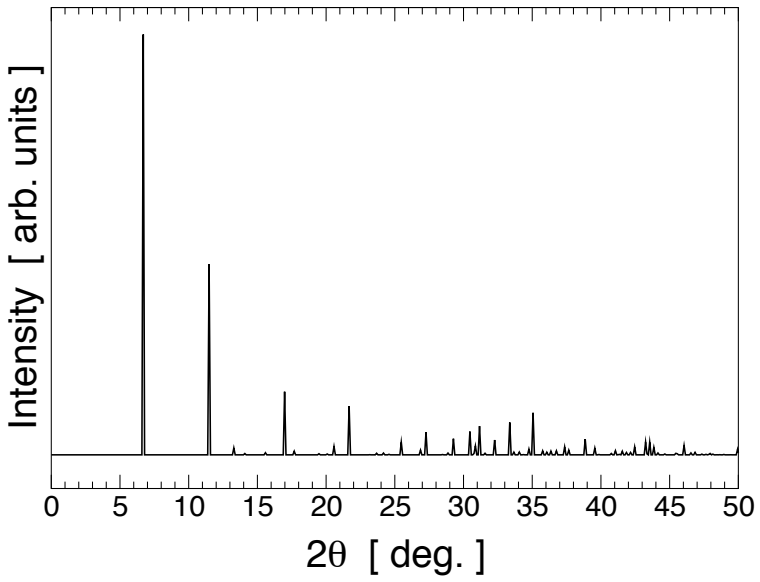

FIG. 4. X-ray powder diffraction pattern for MOF-74-Pt, using a Cu K source.

III. LATTICE PARAMETERS, INTERATOMIC DISTANCES, ADSORPTION ENERGIES, AND ADSORPTION-ENERGY CONTRIBUTIONS

Table II reports the calculated lattice parameters, relevant atomic distances, adsorption energies, and relevant adsorption-energy contributions for MOF-74-$\mathcal{M}$ with $\mathcal{M}$ = Be, Mg, Al, Ca, Sc, Ti, V, Cr, Mn, Fe, Co, Ni, Cu, Zn, Sr, Zr, Nb, Ru, Rh, Pd, La, W, Os, Ir, and Pt. In Table III we compare our computed data with available experimental and computational data.

TABLE II. Computed lattice constants a and c (in Å) for MOF-74-$\mathcal{M}$ after absorption of six H_2, CO_2, CH_4, and H_2O molecules. Absorption energy ΔE and deformation energies $\delta E_{\rm MOF}$ and $\delta E_{\rm M}$ (in kJ mol^{-1}) are also reported. $\mathcal{M}$-X represents the atomic distance (in Å) from the metal ion to the closest atom of the adsorbed molecule.

	H_2						CO_2						CH_4						H_2O					
$\mathcal{M}$	a	c	$\mathcal{M}$-X	ΔE	$\delta E_{\rm MOF}$	$\delta E_{\rm M}$	a	c	$\mathcal{M}$-X	ΔE	$\delta E_{\rm MOF}$	$\delta E_{\rm M}$	a	c	$\mathcal{M}$-X	ΔE	$\delta E_{\rm MOF}$	$\delta E_{\rm M}$	a	c	$\mathcal{M}$-X	ΔE	$\delta E_{\rm MOF}$	$\delta E_{\rm M}$
Be	25.518	6.774	3.311	−16.5	0.4	−0.8	25.413	6.649	3.778	−60.2	4.2	−18.1	25.413	6.649	3.544	−40.2	0.9	−5.8	25.187	6.671	3.835	−41.4	2.3	−4.0
Mg	26.056	6.897	2.853	−15.8	0.3	−0.7	25.944	6.852	2.398	−53.4	1.2	−6.0	25.944	6.852	2.648	−37.0	1.3	−4.6	25.943	6.870	2.232	−73.2	4.2	−5.0
Al	25.535	6.486	2.320	−19.8	−0.9	−0.3	24.988	6.642	1.807	−118.4	126.6	207.7	25.413	6.649	2.656	−38.2	1.0	−4.6	25.480	6.503	2.010	−135.7	23.6	−1.1
Ca	25.122	7.650	3.269	−18.7	1.2	−0.4	24.598	7.208	2.621	−57.0	1.7	−10.0	25.492	7.538	2.809	−40.1	−5.2	0.8	26.233	7.505	2.485	−87.1	9.1	−2.2
Sc	23.424	7.363	3.473	−19.6	0.6	−0.6	23.450	7.319	3.746	−53.0	1.5	−8.5	23.840	7.272	2.905	−45.3	1.3	−7.0	25.786	7.126	2.265	−113.1	16.5	−0.9
Ti	21.503	7.023	3.513	1.4	12.0	8.0	22.696	7.257	4.400	−49.4	5.0	−12.6	22.606	7.269	3.543	−39.9	5.8	−9.6	22.583	7.274	4.283	−50.7	6.0	−35.7
V	25.417	8.135	3.471	−20.0	−0.6	−0.4	26.026	6.827	2.257	−52.7	7.5	−1.0	26.007	6.934	2.378	−43.3	2.4	−3.2	26.038	6.900	2.185	−110.9	6.1	−0.9
Cr	26.206	6.308	3.767	−19.8	0.2	−0.5	26.053	6.529	3.826	−52.9	1.0	−4.4	25.987	6.500	2.975	−37.8	1.2	−5.9	26.955	5.802	2.499	−51.1	12.4	−2.4
Mn	26.316	6.928	3.000	−19.0	0.5	−0.3	26.170	7.064	2.755	−53.7	2.6	−3.6	26.170	7.064	2.694	−43.2	0.5	−4.9	26.244	7.011	2.341	−73.1	11.3	−2.7
Fe	25.994	6.810	3.461	−19.8	−0.2	−0.4	25.854	6.639	3.705	−51.2	1.4	−5.4	25.854	6.639	3.131	−39.8	1.5	−5.9	31.031	4.128	2.142	−129.7	30.1	−4.0
Co	26.109	7.004	3.387	−19.8	0.5	−0.4	25.990	6.870	2.531	−45.8	1.5	−5.4	25.628	6.159	2.707	−37.4	0.8	−5.1	26.252	6.582	2.254	−71.7	12.1	−3.0
Ni	25.740	5.997	3.415	−19.1	0.3	−1.5	25.628	6.159	2.524	−47.4	0.6	−6.1	25.628	6.159	3.033	−36.0	0.6	−6.3	26.062	5.904	2.183	−60.6	3.9	−3.4
Cu	—[e]	—	—	—	—	—	25.990	6.870	2.973	−42.9	0.8	−0.6	26.213	6.094	2.919	−39.7	0.6	−5.1	30.246	4.256	2.233	−90.3	−18.1	8.8
Zn	26.108	6.816	2.745	−20.9	0.4	−1.5	26.159	6.570	3.826	−52.4	0.7	−3.1	26.177	6.472	2.851	−40.1	0.6	−3.3	26.769	5.841	2.228	−73.9	3.4	−3.8
Sr	27.192	6.544	3.250	−18.6	1.2	−0.4	27.513	6.559	2.980	−49.7	5.2	−1.7	26.827	6.765	2.831	−43.9	−0.2	−5.1	30.973	4.447	2.505	-153.6	31.2	0.8
Zr	23.329	7.517	3.651	−17.8	0.2	−0.9	23.060	7.552	4.265	−52.0	1.7	−11.9	22.984	7.566	3.537	−43.8	2.1	−8.4	23.298	7.260	2.370	−90.3	29.7	−3.3
Nb	26.905	3.031	2.911	−20.7	−0.2	0.2	27.262	6.520	2.361	−89.1	5.5	−0.6	26.171	6.525	2.533	−44.5	4.9	−1.0	27.255	6.559	2.325	−124.5	3.6	−1.8
Ru	27.112	6.261	3.539	−20.5	−0.3	−0.7	27.092	5.901	3.794	−49.5	1.8	−2.5	27.065	5.927	3.220	−38.5	1.7	−3.8	25.970	4.947	3.163	−77.5	15.0	−0.1
Rh	25.936	7.120	3.650	−20.8	−0.5	−0.4	25.515	6.827	3.968	−52.5	1.3	−7.1	25.545	6.818	2.911	−36.1	1.0	−6.2	25.782	6.798	3.882[f]	−50.5	0.6	−2.9
Pd	26.271	6.138	4.029	−19.5	0.1	−0.7	26.611	6.384	3.591	−51.3	0.2	−2.3	26.424	6.413	3.102	−37.4	0.6	−5.7	26.721	6.360	3.447[f]	−46.1	0.7	−2.6
La	26.9673	7.099	2.977	−20.2	−0.9	−0.7	27.254	6.223	2.844	−90.0	6.2	6.6	26.672	6.369	2.830	−40.9	0.8	−4.9	27.460	5.935	2.661	−105.2	17.1	0.3
W	26.777	6.336	3.126	−21.9	−0.9	−0.4	26.926	6.134	4.030	−52.0	0.5	−5.2	27.052	6.204	2.172	−40.8	1.7	−5.6	27.126	6.281	2.231	−133.2	7.9	0.2
Os	26.294	6.480	4.121	−19.1	0.3	−10.0	26.319	4.953	4.250	−58.8	1.1	−16.2	—[e]	—	—	—	—	—	26.134	4.973	3.488[f]	−50.5	4.7	−1.7
Ir	26.021	7.276	3.676	−20.4	−0.4	−0.4	21.916	6.917	3.907	−55.1	8.8	−18.0	25.654	6.839	3.098	−36.8	1.2	−6.1	25.956	6.804	3.915[f]	−49.0	1.2	−2.8
Pt	26.597	6.351	3.790	−19.3	−0.4	−0.6	26.527	6.468	3.966	−52.2	0.2	−2.5	26.276	6.541	3.237	−36.1	1.0	−5.9	26.623	6.471	4.239[f]	−45.1	1.0	−2.4

[a]Experimental data. [b]Computational DFT-LDA data. [c]Computational DFT-PBE+D Grimme data. [d]Computational DFT-B3LYP+D Grimme data.
[e]Simulation considered not converged since we observe unphysical dissociation due to huge structural strains. [f]Here we give the distance between the site labeled as 2$^{\rm nd}$ in Fig. 4 in the main manuscript and the closest atom of the bound molecule.

TABLE III. Same as Table II, but here we compare our calculated data with experimental and other computational data where available. For each metal $\mathcal{M}$ our calculated values from Table II are given in the first line and the values we compare to are given in the line(s) underneath.

	H_2				CO_2				CH_4				H_2O			
$\mathcal{M}$	a	c	$\mathcal{M}$-X	ΔE	a	c	$\mathcal{M}$-X	ΔE	a	c	$\mathcal{M}$-X	ΔE	a	c	$\mathcal{M}$-X	ΔE
Mg	26.056	6.897	2.853	–15.8	25.944	6.852	2.398	–53.4	25.944	6.852	2.648	–37.0	25.943	6.870	2.232	–73.2
	—	—	—	$-10.1^{a,3}$	$25.824^{a,7}$	$6.8904^{a,7}$	$2.283^{a,7}$	$-47.0^{a,8}$	$25.850^{a,1}$	$6.9070^{a,1}$	—	—	—	—	—	—
	—	—	$2.54^{b,3}$	$-24.8^{b,3}$	—	—	$2.45^{c,2}$	$-41.4^{c,2}$	—	—	$2.64^{b,1}$	$-33.8^{b,1}$	—	—	—	$-78.8^{d,9}$
Ca	25.122	7.650	3.269	–18.7	24.598	7.208	2.621	–57.0	25.492	7.538	2.809	–40.1	26.233	7.505	2.485	–87.1
	—	—	—	—	—	—	$2.65^{c,2}$	$-36.5^{c,2}$	—	—	—	—	—	—	—	—
Sc	23.424	7.363	3.473	–19.6	23.450	7.319	3.746	–53.0	23.840	7.272	2.905	–45.3	25.786	7.126	2.265	–113.1
	—	—	—	—	—	—	$2.58^{c,2}$	$-40.2^{c,2}$	—	—	—	—	—	—	—	—
Ti	21.503	7.023	3.513	1.4	22.696	7.257	4.400	–49.4	22.606	7.269	3.543	–39.9	22.583	7.274	4.283	–50.7
	—	—	—	—	—	—	$2.44^{c,2}$	$-50.1^{c,2}$	—	—	—	—	—	—	—	—
V	25.417	8.135	3.471	–20.0	26.026	6.827	2.257	–52.7	26.007	6.934	2.378	–43.3	26.038	6.900	2.185	–110.9
	—	—	—	—	—	—	$2.34^{c,2}$	$-47.3^{c,2}$	—	—	—	—	—	—	—	—
Cr	26.206	6.308	3.767	–19.8	26.053	6.529	3.826	–52.9	25.987	6.500	2.975	–37.8	26.955	5.802	2.499	–51.1
	—	—	—	—	—	—	$2.86^{c,2}$	$-21.5^{c,2}$	—	—	—	—	—	—	—	—
Mn	26.316	6.928	3.000	–19.0	26.170	7.064	2.755	–53.7	26.170	7.064	2.694	–43.2	26.244	7.011	2.341	–73.1
	—	—	—	$-4.7,^{a,3}$	—	—	—	—	—	—	—	—	—	—	—	—
	—	—	$2.77^{b,3}$	$-22.4^{b,3}$	—	—	$2.66^{c,2}$	$-28.8^{c,2}$	—	—	$2.73^{b,1}$	$-29.8^{b,1}$	—	—	—	—
Fe	25.994	6.810	3.461	–19.8	25.854	6.639	3.705	–51.2	25.854	6.639	3.131	–39.8	31.031	4.128	2.142	–129.7
	—	—	—	—	—	—	$3.01^{c,2}$	$-25.3^{c,2}$	—	—	—	—	—	—	—	—
Co	26.109	7.004	3.387	–19.8	25.990	6.870	2.531	–45.8	25.628	6.159	2.707	–37.4	26.252	6.582	2.254	–71.7
	—	—	—	$-10.7^{a,3}$	—	—	—	—	—	—	—	—	—	—	—	—
	—	—	$2.31^{b,3}$	$-35.6^{b,3}$	—	—	$2.72^{c,2}$	$-29.2^{c,2}$	—	—	$2.74^{b,1}$	$-29.7^{b,1}$	—	—	—	—
Ni	25.740	5.997	3.415	–19.1	25.628	6.159	2.524	–47.4	25.628	6.159	3.033	–36.0	26.062	5.904	2.183	–60.6
	—	—	—	$-10.7^{a,3}$	$25.784^{a,10}$	$6.7474^{a,10}$	$2.29^{a,10}$	$-41.0^{a,11}$	—	—	—	—	$25.9783^{a,5}$	$6.6883^{a,5}$	$2.08^{a,5}$	—
	—	—	$2.13^{b,3}$	$-39.0^{b,3}$	—	—	$2.92^{c,2}$	$-23.7^{c,2}$	—	—	$2.72^{b,1}$	$-34.8^{b,1}$	—	—	—	—
Cu	—[e]	—	—	—	25.990	6.870	2.973	–42.9	26.213	6.094	2.919	–39.7	30.246	4.256	2.233	–90.3
	—	—	—	—	—	—	$2.86^{c,2}$	$-21.5^{c,2}$	—	—	—	$-34.7^{b,1}$	—	—	—	—
Zn	26.108	6.816	2.745	–20.9	26.159	6.570	3.826	–52.4	26.177	6.472	2.851	–40.1	26.769	5.841	2.228	–73.9
	$25.854^{a,12}$	$6.851^{a,12}$	—	$-8.8^{a,3}$	—	—	—	—	—	—	—	—	—	—	—	—
	—	—	$2.13^{b,3}$	$-22.0^{b,3}$	—	—	$2.71^{c,2}$	$-29.8^{c,2}$	—	—	$2.72^{b,1}$	$-29.7^{b,1}$	$26.212^{d,9}$	$6.989^{d,9}$	$2.125^{d,9}$	$-64.0^{d,9}$

[a]Experimental data. [b]Computational DFT-LDA data. [c]Computational DFT-PBE+D Grimme data. [d]Computational DFT-B3LYP+D Grimme data.
[e]Simulation considered not converged since we observe unphysical dissociation due to huge structural strains.

Figure 5 shows the molecular aggregation found after full relaxation of MOF-74-$\mathcal{M}$ with $\mathcal{M}$ = Be, Ca, Cr, and Os, once CO_2 molecules are adsorbed in the nano-pore. The atom arrangement shown in Fig. 5 clearly demonstrates that the metal ions are not exposed in the pore anymore, inducing a progressive desorption of the adsorbates, which are now agglomerated in the middle of the channel.

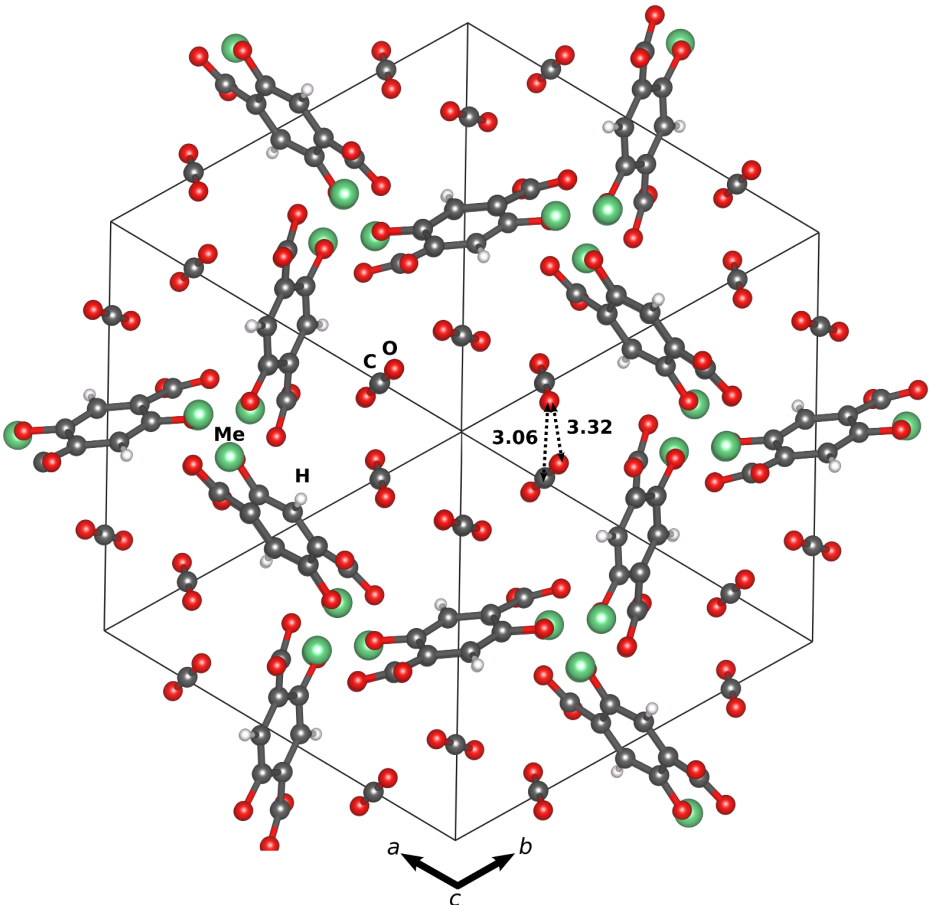

FIG. 5. CO_2 absorbed in MOF-74-$\mathcal{M}$ with $\mathcal{M}$ = Be, Ca, Cr, and Os. Bond lengths (in Å), depicted as dashed lines, refer to the case of MOF-74-Be, but are comparable to the other cases.

Figure 6 clearly shows the chemi-adsorption of CO_2 in MOF-74-Al, in which the oxygen of the adsorbate engages the Al species, whereas the C atom of CO_2 establishes a strong interaction with the C atoms of the benzene rings (i.e. the linkers). Note that the strong interaction of the C atom of CO_2 with the C atoms of the benzene rings disrupts the typical linear symmetry of CO_2.

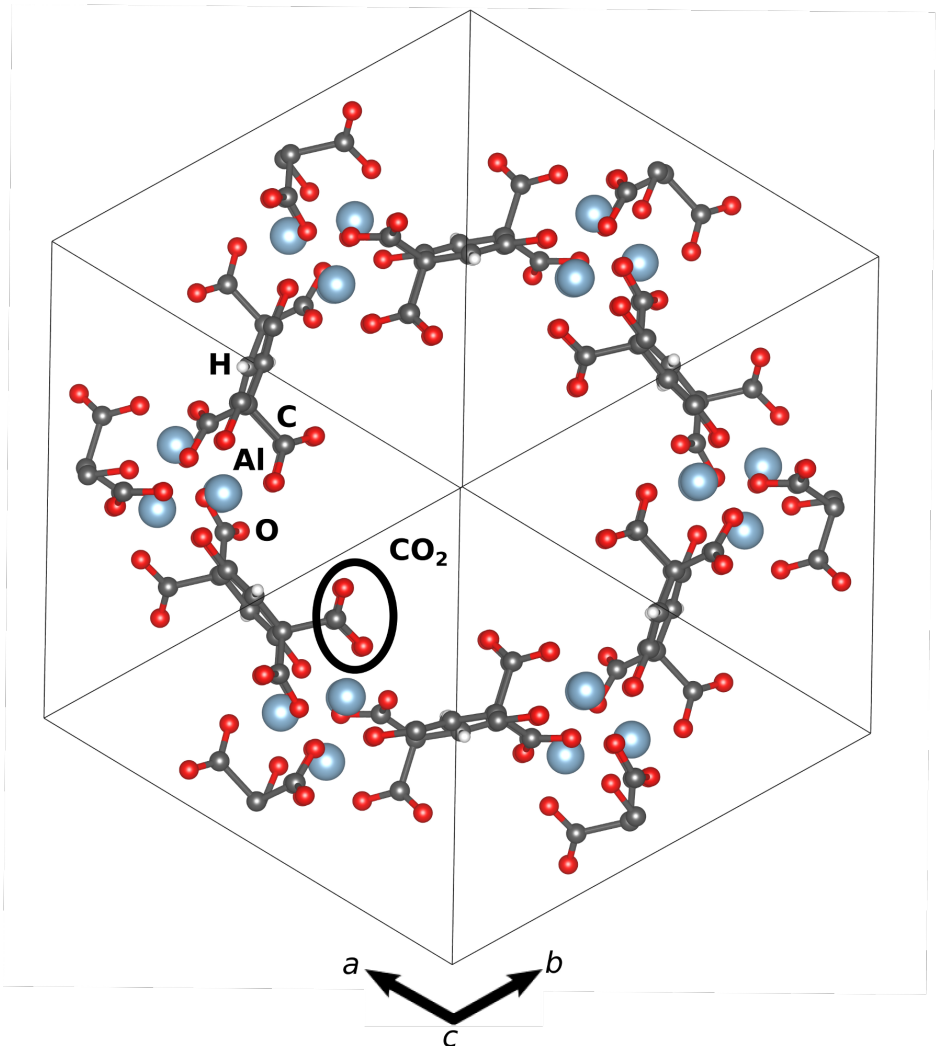

FIG. 6. MOF-74-Al with CO_2 adsorbed at all metal sites. Notice the strong deviation of the bound CO_2 from its typical linear structure.

A strong chemi-adsorption is also observed for MOF-74-La in Fig. 7. From this figure we see that CO_2 is tightly bound via its oxygen atoms to the La species, introducing a significant structural reconstruction.

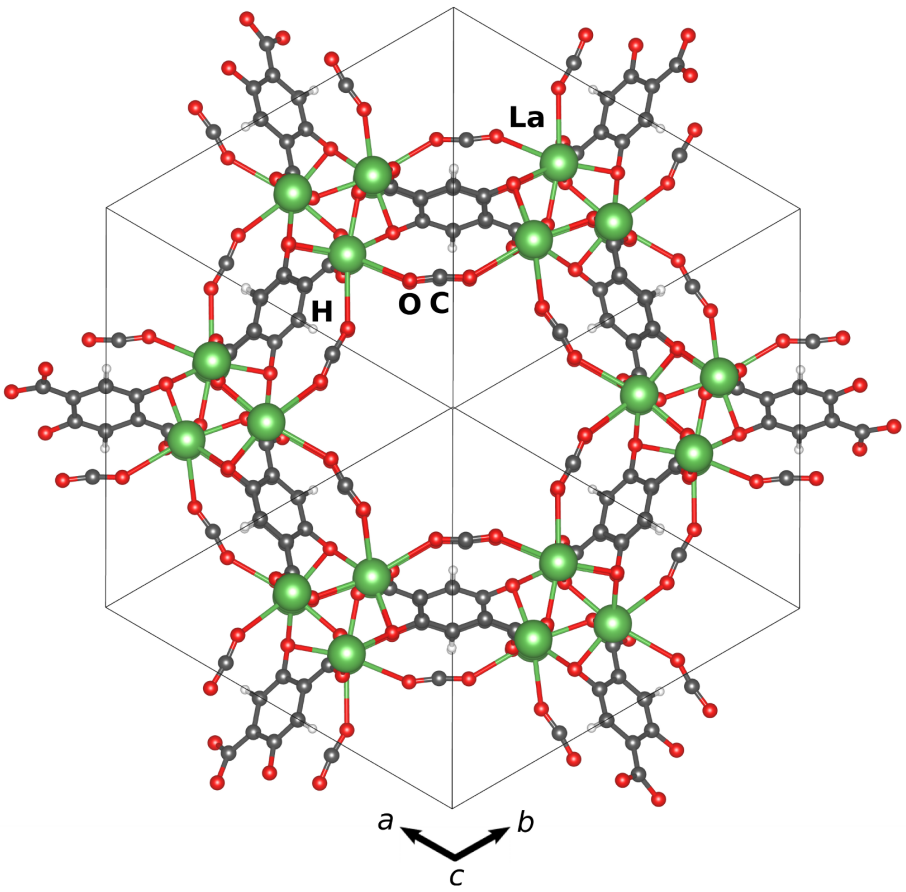

FIG. 7. MOF-74-La with CO_2 adsorbed between all metal sites.

IV. DENSITY OF STATES FOR SELECTED CASES OF WATER IN MOF-74-$\mathcal{M}$

Figures 8, 9, 10, 11, and 12 depict the projected density of states (pDOS) of the relevant atoms involved in the chemi-absorption of H_2O in MOF-74-Sc, -Al, -V, -Nb, and -La. In each figure we report only the pDOS of the O and H atoms of H_2O, O, and the metal species of MOF-74-$\mathcal{M}$; other atoms are removed for the sake of clarity. Metal states dominate at the Fermi energies of MOF-74-V, -Nb, and -W, as can bee seen in Figs. 10, 11, and 12, demonstrating the metallic nature of some of these materials.

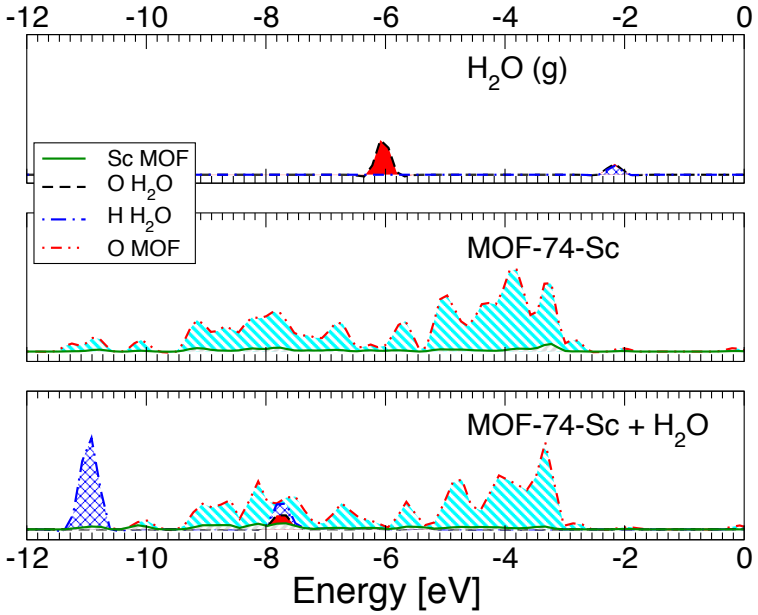

FIG. 8. pDOS for MOF-74-Sc with H_2O, MOF-74-Sc, and H_2O in gas phase. Energies are given in eV with respect to the top of the valence band. Note that up- and down-states are added together.

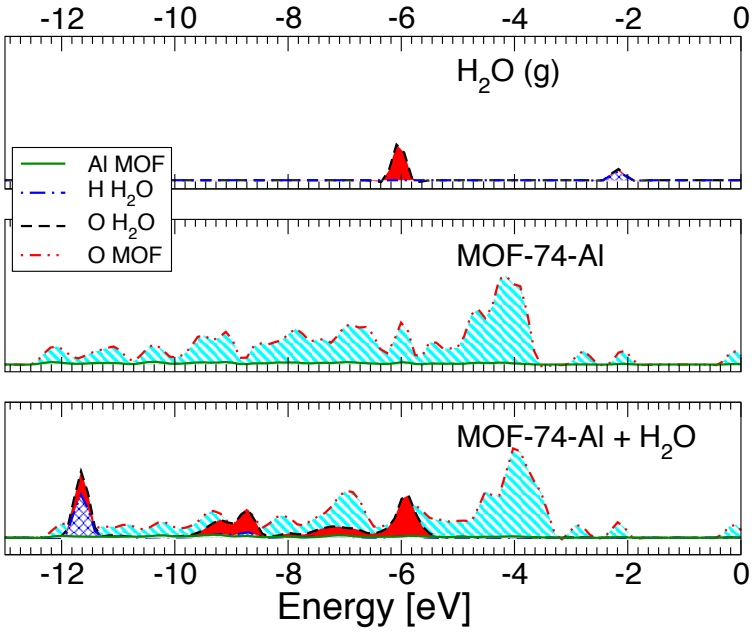

FIG. 9. As in Fig. 8, but here for MOF-74-Al.

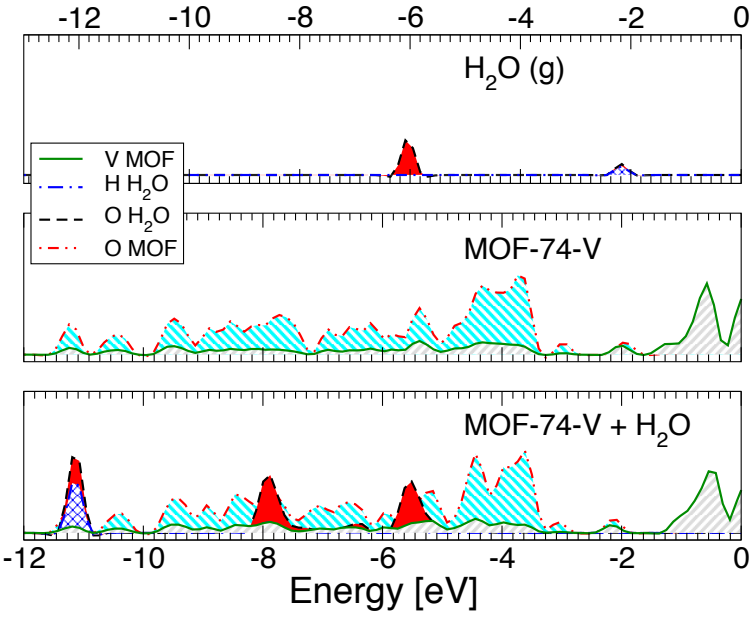

FIG. 10. As in Fig. 8, but here for MOF-74-V.

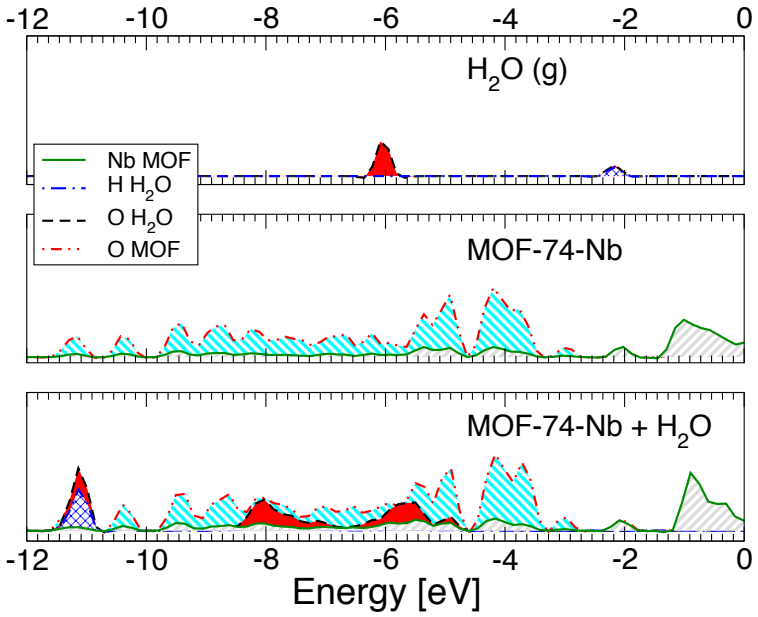

FIG. 11. As in Fig. 8, but here for MOF-74-Nb.

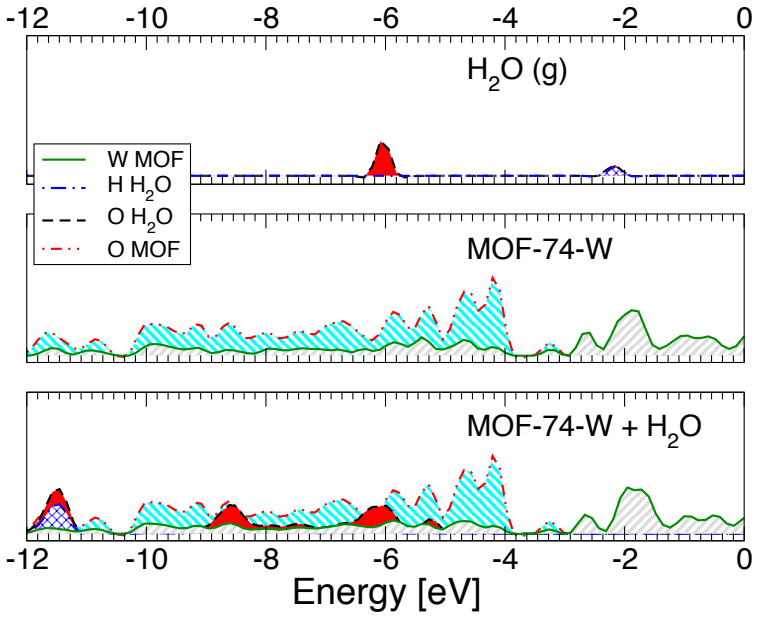

FIG. 12. As in Fig. 8, but here for MOF-74-W.

[1] H. Wu, W. Zhou, and T. Yildirim, J. Am. Chem. Soc. **131**, 4995 (2009).
[2] J. Park, H. Kim, S. S. Han, and Y. Jung, J. Phys. Chem. Lett. **3**, 826 (2012).
[3] W. Zhou, H. Wu, and T. Yildirim, J. Am. Chem. Soc. **46**, 15268 (2008).
[4] E. D. Bloch, W. L. Queen, R. Krishna, C. M. Zadrozny, Brown, and J. R. Long, Science **335**, 1606 (2012).
[5] P. D. C. Dietzel, B. Panella, M. Hirsher, R. Blom, and H. Fjellvåg, Chem. Commun. **9**, 959 (2006).
[6] N. L. Rosi, J. Kim, C. B. Eddaoudi, M. O'Keeffe, and O. M. Yaghi, J. Am. Chem. Soc. **1504**, 127 (2005).
[7] E. L. Queen, C. M. Brown, D. K. Britt, P. Zajdel, M. R. Hudson, and O. M. Yaghi, J. Phys. Chem. C **115**, 24915 (2011).
[8] D. K. Britt, H. Furukawa, B. Wang, T. G. Glover, and O. M. Yaghi, Proc. Nat. Acad. Sci. USA **106**, 20637 (2009).
[9] A. J. Kennedy and L. Valenzano, Prep. Pap.-Am. Chem. Soc., Div. Fuel Chem. **57**, 913 (2012).
[10] P. D. C. Dietzel, R. E. Johnsen, H. Fjellvåg, S. Bordiga, E. Groppo, S. Chavan, and R. Blom, Chem. Commun. **46**, 5125 (2008).
[11] L. Valenzano, B. Civalleri, S. Chavan, G. T. Palomino, C. O. Areán, and S. Bordiga, J. Phys. Chem. C **114**, 11185 (2010).
[12] Y. Liu, C. Kabbour, C. Brown, D. A. Neumann, and C. C. Ahn, Langmuir **24**, 4772 (2008).